# Preparation of Lignin-based Carbon Microporous Materials Using Cesium Chloride and Characterization

Bo Meng , Haichao Li , \* Zezhong Lin , and Chong Wang

A carbon adsorbent material with a specific surface area of 342 m²/g was prepared *via* chemical activation, using lignin as the raw material and CsCl as the activator. The adsorbent's structure was characterized and its performance for methylene blue solution was investigated. Additionally, adsorption experiments of crystalline violet dye were conducted at different temperatures to study the adsorption thermodynamics. The results indicated that the prepared activated carbon material featured a smooth surface with abundant pores. Its adsorption capacity for methylene blue reached 161 mg/g, enabling rapid and efficient adsorption of methylene blue solution. Additionally, it exhibited excellent adsorption performance for crystalline violet solution: at 40 °C, the saturated adsorption capacity reached 243 mg/g with a removal of 93%, and the adsorption process was confirmed to be a spontaneous thermodynamic reaction. The experiments confirmed that CsCl can serve as an activator for activating lignin-based raw materials to prepare carbon samples.

DOI: 10.15376/biores.20.4.10290-10299

Keywords: Lignin; Cesium chloride; Activated carbon

Contact information: Qinghai Minzu University, Qinghai Provincial Key Laboratory of Nanomaterials and Technology, Qinghai Xining 810007, China; \*Corresponding author: lihaichao@yip.163.com

# INTRODUCTION

Lignin is an amorphous aromatic polymer containing oxybenzyl alcohol or its derivative structural units in its molecular structure. It is widely distributed in the tissues of higher vascular plants and represents the only non-petroleum resource in nature that supplies renewable aromatic compounds (Correa et al. 2017). Cellulose, hemicellulose, and lignin are the three main components of biomass, with the content of lignin being second only to that of cellulose but typically higher than that of hemicellulose (Han et al. 2019). Lignin, a major component in papermaking wastewater, not only pollutes the environment but also leads to resource waste (Bergna et al. 2022). In recent years, the wastewater discharge began increasing with the development of the printing and dyeing industry despite improvements in wastewater treatment (Yang et al. 2020). Dyes in water bodies not only affect the photosynthetic activity of aquatic organisms but also exert toxic effects on them (Yu et al. 2022). Activated carbon not only has the advantages of low cost and strong adsorption capacity (Mohamad Said et al. 2023), but it also can be used as a catalyst carrier (Yakub et al. 2022). The preparation of activated carbon using agricultural and forestry wastes as raw materials has become a hot topic in the field of adsorption material research and development (Yang et al. 2022). The production of activated carbon from lignin can realize waste recycling and reduce pollution (Rosas et al. 2017).

Kamwilaisak *et al.* (2022) pretreated lignin *via* H<sub>2</sub>SO<sub>4</sub> hydrolysis prior to activation and carbonization. They also investigated the effects of H<sub>3</sub>PO<sub>4</sub> concentration (0 to 66 wt%)

and impregnation time (0 to 12 h) on activated carbon, where H<sub>3</sub>PO<sub>4</sub> served as the impregnating agent. After 8 h of impregnation and activation at 500 °C, an activated carbon material with a specific surface area of 1650 m<sup>2</sup>/g was obtained. Rowlandson *et al.* (2020) studied two different types of organic solvents for lignin; the resulting activated carbon exhibited a specific surface area exceeding 1000 m<sup>2</sup>/g, possessed certain adsorption properties, and could reasonably adsorb up to 1.8 wt% hydrogen at 1.0 bar and -196 °C. Wei *et al.* (2023) prepared nitrogen-doped activated carbon through self-activation of endogenous alkali using sulfated lignin from black liquor. The obtained activated carbon had a specific surface area of 1120 m<sup>2</sup>/g and a total pore volume of 0.60 cm<sup>3</sup>/g. It showed excellent adsorption capacity, with a maximum adsorption capacity of 374 mg/g when the initial concentration of the methyl orange solution was 175 mg/L.

In this study, lignin was activated *via* chemical activation using CsCl as the activator. The results indicated that CsCl exhibited an activating effect on lignin, and the resulting activated carbon material had a specific surface area of 342 m<sup>2</sup>/g with a methylene blue adsorption capacity of 161 mg/g. This is similar to the relevant previous studies (Zhang *et al.* 2024), which shows that cesium chloride can be used as a new type of activator for preparing activated carbon materials.

### **EXPERIMENTAL**

#### **Materials**

Alkaline lignin and CsCl (analytical grade) were purchased from Shanghai Aladdin Biochemical Technology Co., Ltd. The molecular weight and preparation process of alkaline lignin are unknown. The purchased reagents were used directly without secondary treatment, and deionized water was used in the experiment.

# **Preparation of Activated Carbon**

Lignin powder and cesium chloride (CsCl) were mixed in a crucible at a mass ratio of 5:1, followed by impregnation with 20 mL of deionized water. The crucible was then placed in an oven at 70 °C until completely dry. After drying, it was transferred to a muffle furnace. Under an air atmosphere, the temperature was raised to 600 °C at a heating rate of 10 °C/min and maintained for 2 h to complete the activation, resulting in the product. The product was repeatedly washed with deionized water until the pH value of the filtrate was close to neutral. Subsequently, the activated sample was filtered, dried, ground, and weighed to obtain activated carbon AC600 for subsequent use.

#### **Characterization Methods**

The adsorption capacity of methylene blue was determined with reference to the GB/T12496.10-1999 test method for wood-based activated carbon. The specific surface area (BET) and porosity of the activated carbon were analyzed using a surface area and pore structure analyzer (miniX, McMurray Tic Ltd.) under the conditions of 77 K and nitrogen. The microstructure of the activated carbon was observed *via* a field emission scanning electron microscope (FESEM, SU8010, Hitachi, Japan). A proper amount of activated carbon was adhered to a double-sided adhesive specimen sheet, followed by gold sputtering in a vacuum coater under the conditions: accelerating voltage of 20 kV, acquisition time of 100 s, and scanning interval of 15 mm. X-ray diffraction (XRD) analysis was performed using a Rigaku SmartLab diffractometer (Rigaku, Japan). X-ray

photoelectron spectroscopic (XPS) measurements were carried out on a Thermo Scientific ESCALab 250Xi+ spectrometer (USA), employing 150 W monochromated Al Kα radiation (1,486.6 eV). A 500 μm X-ray spot was used for the analysis, and the base pressure in the analysis chamber was approximately  $3\times10^{-10}$  mbar. For energy calibration, the C1s peak of adventitious carbon at 284.8 eV was typically used as the reference. Fourier transform infrared (FTIR) spectroscopy was performed using a Thermo Fisher Nicolet iS5 spectrometer. Raman spectroscopy was conducted using a Thermo Fisher DxR spectrometer.

# **Dye Adsorption**

Thermodynamic parameters are critical in the adsorption process, as they can predict the spontaneity of adsorption. Based on experimental data at 20 °C (293 K), 30 °C (303 K), and 40 °C (313 K), the thermodynamic parameters for the adsorption of adsorbate on the adsorbent surface were determined. The Gibbs free energy ( $\Delta G^0$ ), enthalpy ( $\Delta H^0$ ), and entropy ( $\Delta S^0$ ) were calculated using the Gibbs and Van't Hoff equations, as shown below,

$$lnK_d = -\frac{\Delta H^0}{RT} + \frac{\Delta S^0}{R'} \tag{1}$$

where R represents the gas constant (8.314 J·mol<sup>-1</sup>·K<sup>-1</sup>), T denotes the adsorption temperature in Kelvin,  $K_d$  is the partition coefficient,  $q_e$  signifies the equilibrium adsorption capacity (mg·g<sup>-1</sup>), and  $c_e$  stands for the equilibrium concentration of the adsorbate (mg·L<sup>-1</sup>).

$$K_d = \frac{q_e}{c_a} \tag{2}$$

$$\Delta G^0 = -RT ln K_d \tag{3}$$

Each group of adsorption tests was performed in five parallel replicates, with the average value calculated for analysis.

#### RESULTS AND DISCUSSION

Samples from the five experimental runs were combined into a single composite sample for characterization and subsequent analysis.

# Characterization of Activated Carbon

The specific surface area, together with the pore size structure, is a key parameter of activated carbon and a critical factor influencing the adsorbent's performance. The adsorption-desorption isotherms and pore size distribution of the activated carbon AC600 are presented in Fig. 1, while the specific surface area parameters at different activation temperatures are summarized in Table 1. As shown in Table 1, the activated carbon sample prepared *via* CsCl activation of lignin at 600 °C exhibited a specific surface area of 342 m<sup>2</sup>/g, a pore volume of 0.172 cm<sup>3</sup>/g, and an average pore size of 2.01 nm. These results indicate that CsCl activation of lignin at 600 °C yielded activated carbon with a relatively high specific surface area and small pore sizes, predominantly in the microporous range.

| Table II Characterization recount of recounted retrated Carbon Campie |              |                                    |                           |                              |  |  |  |  |  |  |
|---|--------------|------------------------------------|---------------------------|------------------------------|--|--|--|--|--|--|
| Sample  | Yield<br>(%) | Specific<br>Surface Area<br>(m²/g) | Pore<br>Volume<br>(cm³/g) | Average<br>Pore Size<br>(nm) | Adsorption Capacity of<br>Methylene Blue<br>(mg/g) |  |  |  |  |  |
| Lignin-based  | 6.46         | 342                                | 0.172                     | 2.01                         | 161  |  |  |  |  |  |

**Table 1.** Characterization Results of Produced Activated Carbon Sample

According to the IUPAC 2015 classification (Li *et al.* 2013), the adsorption-desorption isotherm (Fig. 1(a)) belongs to Type I(b). It is characterized by a steep slope in the low relative pressure region, and N<sub>2</sub> adsorption gradually reaches equilibrium with increasing relative pressure, primarily due to strong adsorbate-adsorbent interactions. The hysteresis loop is nearly parallel to the adsorption isotherm and rises vertically, indicating a pore structure composed of interconnected particles.

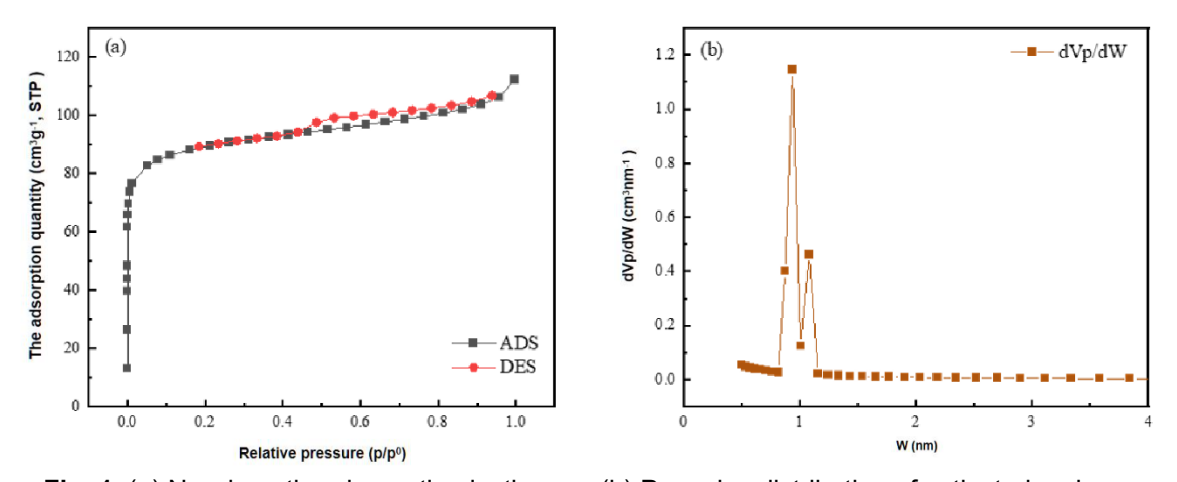


Fig. 1. (a) N<sub>2</sub> adsorption-desorption isotherms, (b) Pore size distribution of activated carbon

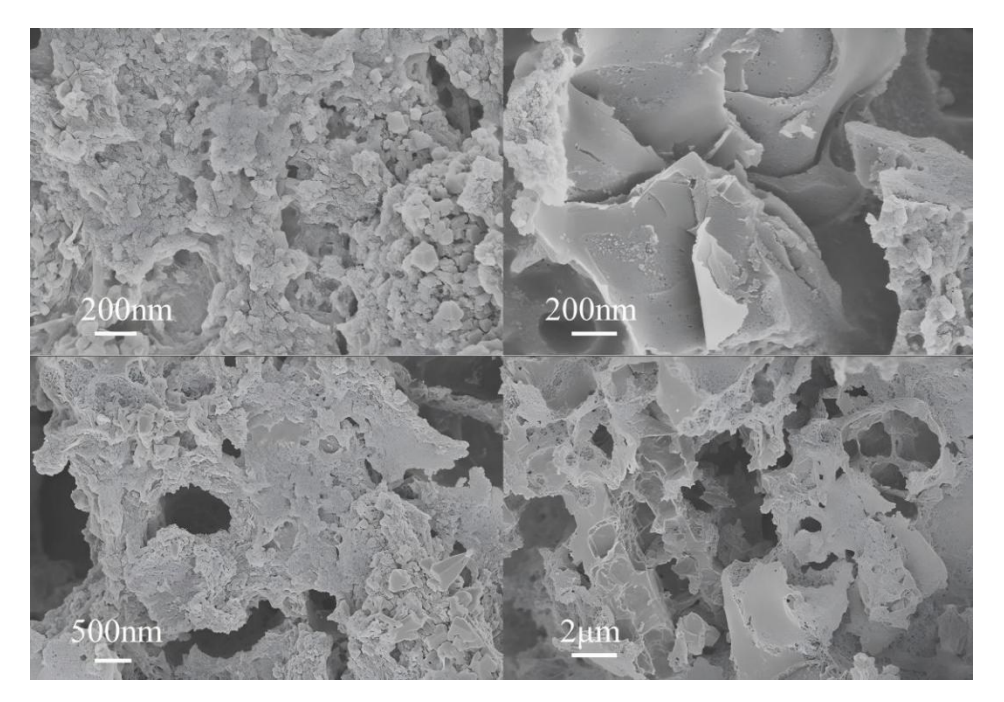


Fig. 2. SEM images of AC600

As shown in Fig. 1(b), the pore size distribution of the activated carbon is dominated by peaks at 0.81 and 1.15 nm, confirming that the material had extremely fine pores and could be classified as microporous.

The surface morphology of the activated carbon was characterized by scanning electron microscopy (SEM), and the results are shown in Fig. 2. As illustrated in the figure, the activated carbon is composed of interconnected particles with abundant pores. With the increase of temperature, the lignin undergoes carbonization and activation, leading to the formation of pores with various shapes and sizes.

Figures 3(a-b) display the Raman and XRD spectra of lignin-derived activated carbon AC600, respectively. As shown in Fig. 3(a), two distinct broad peaks at 1350 and 1580 cm<sup>-1</sup> correspond to the D and G bands, respectively. The D band is associated with defects, disorder, and graphite-like amorphous structures, while the G band corresponds to lattice vibrations of graphitic carbon. Generally, the graphitization degree of carbon increases with rising heat treatment temperature (Wu *et al.* 2023). The ID/IG ratio of AC600 was 0.9302, indicating that the lignin-derived activated carbon had a high degree of graphitization (Rajagopal *et al.* 2016). In the XRD pattern (Fig. 3(b)), broad diffraction peaks at  $2\theta = 24^{\circ}$  and 44° are indexed to the (002) and (100) planes of graphene, respectively (Lawal *et al.* 2024). The (002) plane corresponds to microcrystals—specifically aromatic microcrystals formed by condensed aromatic nuclei, consistent with the conventional definition of microcrystals. The (100) plane is related to the condensation degree of aromatic rings (*i.e.*, the size of aromatic carbon sheets), confirming the presence of a microcrystalline structure in the lignin-derived activated carbon (Fernandez-Ruiz *et al.* 2018). These results are consistent with the Raman analysis.

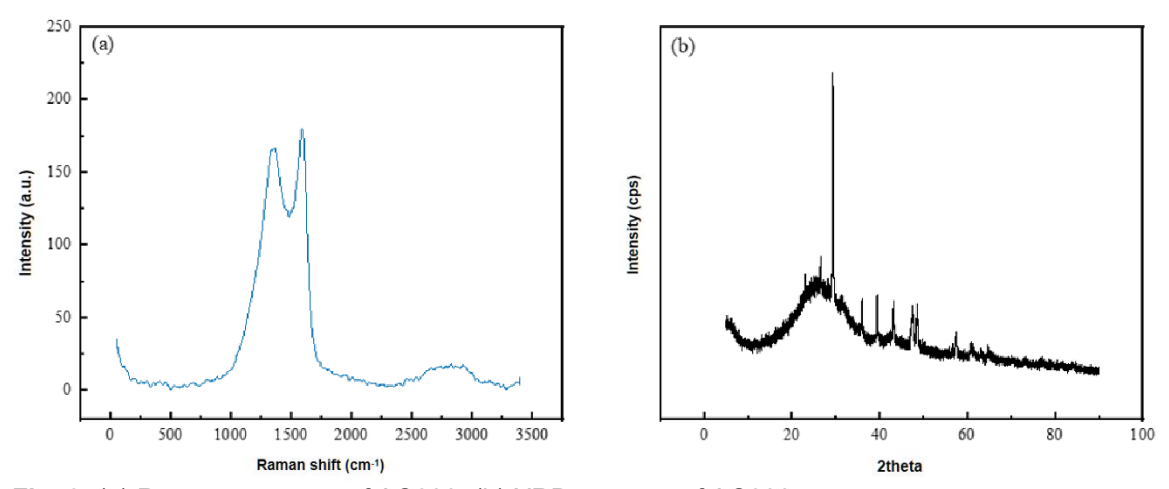
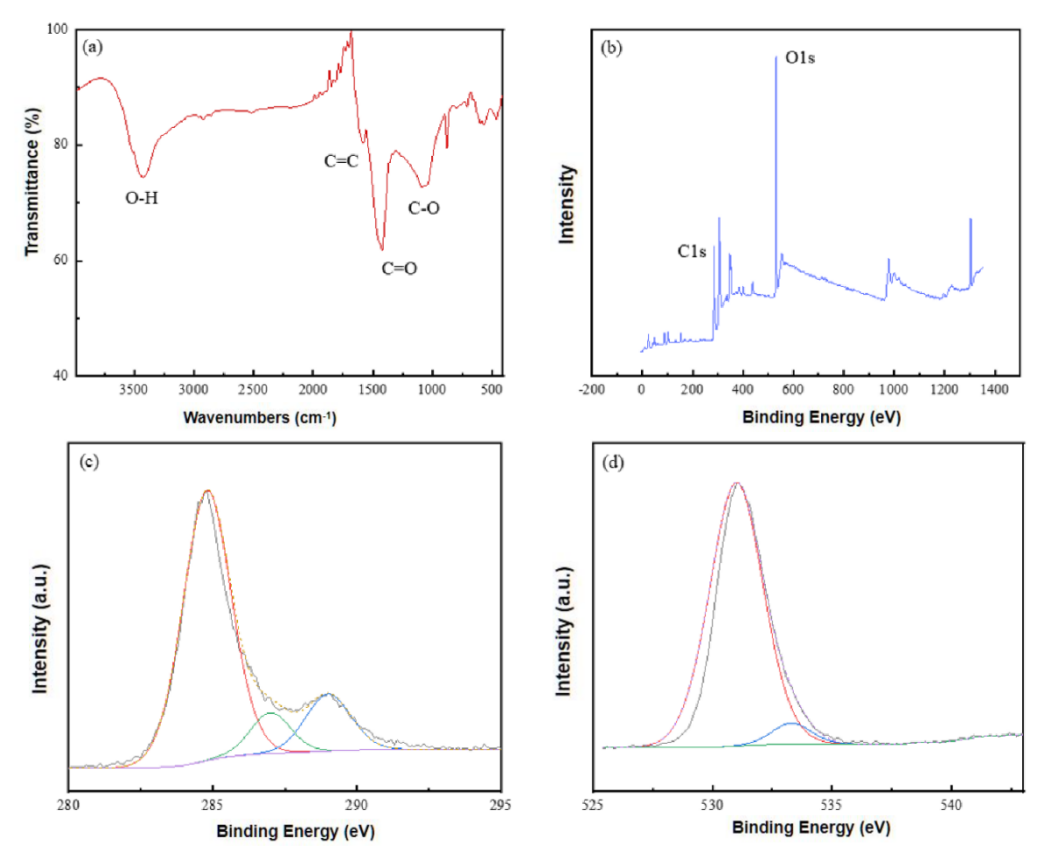


Fig. 3. (a) Raman spectrum of AC600, (b) XRD patterns of AC600

The FTIR spectrum of AC600 is presented in Fig. 4(a), revealing the presence of functional groups such as C-O, C=O, C=C, and O-H. Previous studies have demonstrated that oxygen-containing functional groups influence the chemisorption capacity of activated carbon (Mohamad Nasran Nasehir Khan *et al.* 2023). As shown in Figs. 4(b-c), deconvolution of the C1s XPS spectrum yielded three peaks at 284.8 eV, 287.0 eV, and 289.1 eV, corresponding to C=C, C-O, and C=O bonds, respectively (Luis M. Cotoruelo *et al.* 2007). Deconvolution of the O1s spectrum revealed two peaks at 531.0 eV and 533.2 eV, assigned to C=O and C-O groups (Jun Wang *et al.* 2017). These results are consistent with the FTIR data.



**Fig. 4.** (a) FTIR of AC600, The XPS wide scan spectra (b) of AC600, C1s spectra (c), O1s spectra, and (d) of AC600

# **Adsorption Thermodynamics**

Three 0.1 g portions of activated carbon AC600 were weighed into 250 mL conical flasks, with adsorption temperatures set at 20 °C, 30 °C, and 40 °C, respectively.

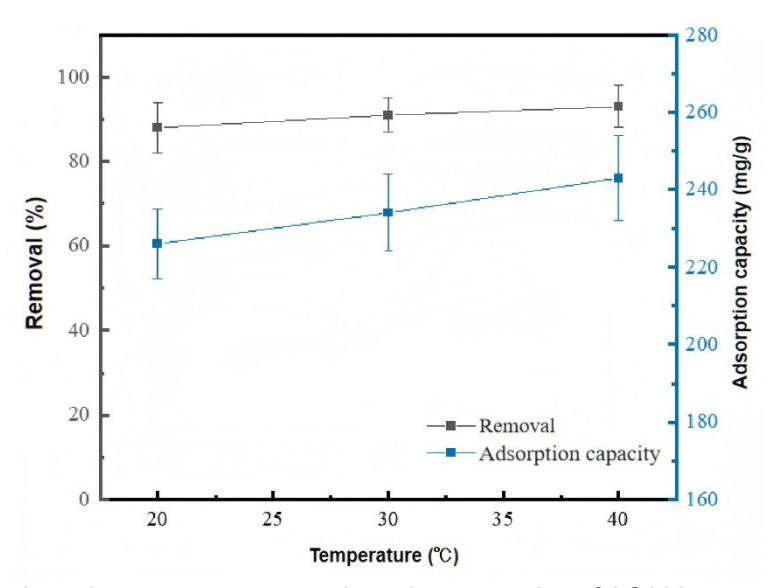


Fig. 5. Effect of adsorption temperature on adsorption properties of AC600

The mixtures were shaken in a water-bath shaker at 180 r/min for 20 min after the dropwise addition of 100 mg/L crystal violet solution. Following adsorption, the samples were centrifuged for phase separation. An appropriate volume of supernatant was collected to measure its absorbance, from which the adsorption capacity and removal rate were calculated. The results are presented in Fig. 5.

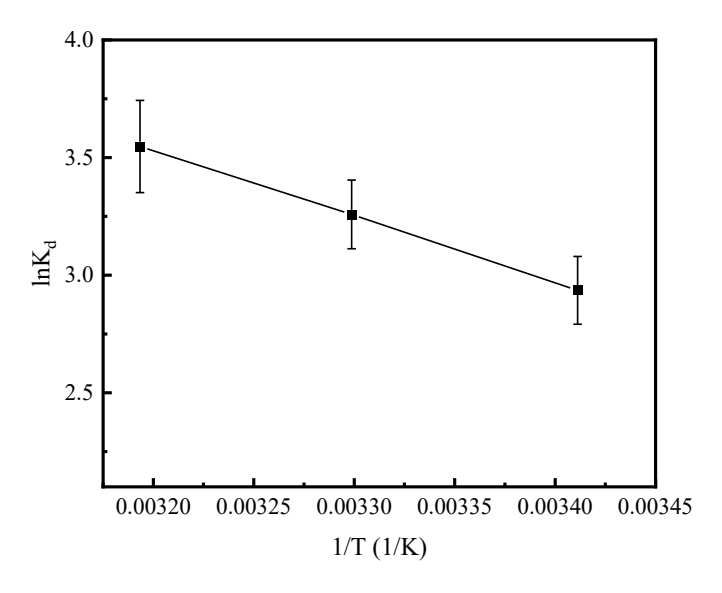


Fig. 6. Van't Hoff diagram of adsorption of crystal violet by AC600

The thermodynamic parameters for the adsorption of crystal violet by AC600 are summarized in Table 2, and the corresponding Van't Hoff plot is depicted in Fig. 6. All calculated  $\Delta G^0$  values were negative, confirming that the adsorption of crystal violet onto AC600 was a spontaneous process (Qu *et al.* 2019). The positive  $\Delta H^0$  value indicates an endothermic adsorption mechanism, while the positive  $\Delta S^0$  suggests an increase in system disorder during adsorption. These results are consistent with the characteristics of a physical adsorption process.

**Table 2.** Thermodynamic Parameters Values for the Adsorption of Crystal Violet onto AC600

| Temperature | Thermodynamics |  |                                      |  |  |  |
|-------------|----------------|--|--------------------------------------|--|--|--|
| (°C)        | $lnK_d$        | $\Delta G^{\theta}(KJ \cdot mol^{-1})$ | $\Delta H^{\theta}(KJ\cdotmol^{-1})$ | $\Delta S^{\theta}(J \cdot mol^{-1} \cdot K^{-1})$ |  |  |
| 20 °C       | 2.93           | -7.15                                  |                                      |  |  |  |
| 30 °C       | 3.26           | -8.21                                  | 23.4                                 | 104.3  |  |  |
| 40 °C       | 3.55           | -9.24                                  |                                      |  |  |  |

# CONCLUSIONS

1. In this study, lignin powder was activated with CsCl at 600 °C. Experimental results indicate that CsCl effectively activated the lignin, yielding activated carbon AC600 with a specific surface area of 342 m<sup>2</sup>/g, pore volume of 0.172 cm<sup>3</sup>/g, and average pore size of 2.01 nm.

- 2. The AC600 material had a methylene blue adsorption capacity of 161 mg/g. Additionally, AC600 showed excellent adsorption performance for crystal violet, achieving a saturated adsorption capacity of 243 mg/g at 40 °C with a removal percent of 93%.
- 3. Thermodynamic analysis showed that the adsorption process of AC600 was spontaneous and endothermic. These findings demonstrate that CsCl can serve as an effective activator for preparing activated carbon from lignocellulosic feedstocks.

# **ACKNOWLEDGMENTS**

This work was supported by the Central Guidance Fund for Local Science and Technology Development (2025-ZY-050).

# REFERENCES CITED

- Bergna, D., Varila, T., Romar, H., and Lassi, U. (2022). "Activated carbon from hydrolysis lignin: Effect of activation method on carbon properties," *Biomass and Bioenergy* 159, article 106387. DOI: 10.1002/cssc.202201284
- Correa, C. R., Stollovsky, M., Hehr, T., Rauscher, Y., Rolli, B., and Kruse, A. (2017). "Influence of the carbonization process on activated carbon properties from lignin and lignin-rich biomasses," *ACS Sustainable Chemistry and Engineering* 5(9), 8222-8233. DOI: 10.1021/acssuschemeng.7b01895
- Cotoruelo, L. M., Marqués, M. D., Rodríguez-Mirasol, J., Cordero, T., and Rodríguez, J. J. (2007). "Adsorption of aromatic compounds on activated carbons from lignin: Equilibrium and thermodynamic study," *Industrial and Engineering Chemistry Research* 46(14), 4982-4990. DOI: 10.1021/ie061415h
- Fernandez-Ruiz, C., Bedia, J., Bonal, P., Rodriguez, J. J., and Gómez-Sainero, L. M. (2018). "Chloroform conversion into ethane and propane by catalytic hydrodechlorination with Pd supported on activated carbons from lignin," *Catalysis Science and Technology* 8, 3926-3935. DOI: 10.1039/c8cy00461g
- GB/T 12496.10 (1999). "Teat methods of wooden activated carbon Determination of methylene blue adsorption," Standardization Administration of China, Beijing, China.
- Han, J., Jeong, S.-Y., Lee, J. H., Choi, J. W., Lee, J.-W., and Roh, K. C. (2019). "Structural and electrochemical characteristics of activated carbon derived from lignin-rich residue," *ACS Sustainable Chemistry and Engineering* 7(2), 2471-2482. DOI: 10.1021/acssuschemeng.8b05351
- Kamwilaisak, K., Siripanee, S., Jutakridsada, P., Pimsawat, N., Chokesawatanakit, N., Rittiwut, K., Theerakulpisut, S., Sillanpääe, M., and Chindaprasirt, P. (2022). "Porosity enhancement of activated carbon by hydrolyzed lignin from black liquor," *Clean Technologies and Environmental Policy* 24, 2517-2530. DOI: 10.1007/s10098-022-02331-z.
- Khan, M. N., Yusop, M. F. M., Latiff, M. F. P. M., and Ahmad, M. A. (2023). "Alteration of Tecoma chip wood waste into microwave-irradiated activated carbon for amoxicillin removal: Optimization and batch studies," *Arabian Journal of Chemistry* 16(10), article 105110. DOI: 10.1016/j.arabjc.2023.105110

- Lawal, M., Oyedepo, O. J., Olukanni, E. O., and Omomomi, O. J. (2024). "Evaluation of physical and mineralogical properties of graphite-modified bitumen," *Journal of Civil Engineering, Science and Technology* 15(2), 96-110. DOI: 10.33736/jcest.5859.2024
- Li, X., Zuo, Y., Zhang, Y., Fu, Y., and Guo, Q.-X. (2013). "*In situ* preparation of K2CO3 supported Kraft lignin activated carbon as solid base catalyst for biodiesel production," *Fuel* 113, 435-442. DOI: 10.1016/j.fuel.2013.06.008
- Mohamad Said, K. A., Mohamed Amin, M. A., Yakub, I., Rahman, M. R., Kueh, A. B. H., Hamdan, S., and Rahman, M. (2023). "Methylene blue adsorption mechanism onto palm kernel shell-derived activated carbon: From particle diffusion to site adsorption," *Bioresources* 18(3), 5120-5132. DOI: 10.15376/biores.18.3.5120-5132
- Qu, W., Yuan, T., Yin, G., Xu, S., Zhang, Q., and Su, H. (2019). "Effect of properties of activated carbon on malachite green adsorption," *Fuel* 249, 45-53. DOI: 10.1016/j.fuel.2019.03.058
- Rajagopal, R. R., Aravinda, L. S., Rajarao, R., Bhat, B. R., and Sahajwalla, V. (2016). "Activated carbon derived from non-metallic printed circuit board waste for supercapacitor application," *Electrochimica Acta* 211, 488-498. DOI: 10.1016/j.electacta.2016.06.077
- Rosas, J. M., Ruiz-Rosas, R., Rodríguez-Mirasol, J., and Cordero, T. (2017). "Kinetic study of SO2 removal over lignin-based activated carbon," *Chemical Engineering Journal* 307, 707-721. DOI: 10.1016/j.cej.2016.08.111
- Rowlandson, J. L., Edler, K. J., Tian, M., and Ting, V. P. (2020). "Toward process-resilient lignin-derived activated carbons for hydrogen storage applications," *ACS Sustainable Chemistry and Engineering* 8(5), 2186-2195. DOI: 10.1021/acssuschemeng.9b05869
- Wang, J., Liu, T.-L., Huang, Q.-X., Ma, Z.-Y., Chi, Y., and Yan, J.-H. (2017). "Production and characterization of high quality activated carbon from oily sludge," *Fuel Processing Technology* 162, 13-19. DOI: 10.1016/j.fuproc.2017.03.017.
- Wei, K., Lv, T., Wang, T., Zhou, H., Jiang, Y., Qin, X., and Liu, Z. (2023). "High adsorption of methyl orange by nitrogen-doped activated carbon derived from kraft lignin *via* self-activation," *Surfaces and Interfaces* 42, article 103484. DOI: 10.1016/j.surfin.2023.103484
- Wu, H., Wei, H., Yang, X., Jin, C., Sun, W., Deng, K., Rong, X., Bin, G., and Sun, C. (2023). "Spherical activated carbons derived from resin-microspheres for the adsorption of acetic acid," *Journal of Environmental Chemical Engineering* 11(2), article 109394. DOI: 10.1016/j.jece.2023.109394
- Yakub, I., Kueh, A. B. H., De La O, E. A. P., Rahman, M. R., Barawi, M. H., Abdullah, M. O., Amran, M., Fediuk, R., and Vatin, N. I. (2022). "Employing an artificial neural network in correlating a hydrogen-selective catalytic reduction performance with crystallite sizes of a biomass-derived bimetallic catalyst," *Catalysts* 12 (779), 1-17. DOI: 10.3390/catal12070779
- Yang, H., Han, T., Shi, Z., Sun, Y., Jiang, J., Sandström, L., Jönsson, P. G., and Yang, W. (2022). "*In situ* catalytic fast pyrolysis of lignin over biochar and activated carbon derived from the identical process," *Fuel Processing Technology* 227, article 107103. DOI: 10.1016/j.fuproc.2021.107103
- Yang, Z., Gleisner, R., Mann, D. H., Xu, J., Jiang, J., and Zhu, J. Y. (2020). "Lignin based activated carbon using H<sub>3</sub>PO<sub>4</sub> activation," *Polymers* 12(12), article 2829. DOI: 10.1002/cssc.202201284

- Yu, L., Keffer, D. J., Hsieh, C.-T., Scroggins, J. R., Chen, H., Dai, S., and Harper, D. P. (2022). "Lignin-derived magnetic activated carbons for effective methylene blue removal," *Industrial and Engineering Chemistry Research* 61(32), 11840-11850. DOI: 10.1021/acs.iecr.2c02311
- Zhang, C. L., Li, H. C., and Du, B. X. (2024). "Preparation and characterization of cellulose-based activated carbon by cesium chloride chemical method," *BioResources* 19(1), 1295-1304. DO1:10.15376/biores.19.1.1295-1304

Article submitted: July 11, 2025; Peer review completed: August 1, 2025; Revised version received and accepted: September 15, 2025; Published: October 13, 2025. DOI: 10.15376/biores.20.4.10290-10299